Inorganic Chemistry

ARTICLE

pubs.acs.org/IC

Analogues of the Lavallo−Grubbs Compound $Fe_3(C_8H_8)_3$: Equilateral, Isosceles, and Scalene Metal Triangles in Trinuclear Cyclooctatetraene Complexes $M_3(C_8H_8)_3$ of the First Row Transition Metals (M = Ti, V, Cr, Mn, Fe, Co, and Ni)

Hongyan Wang,*[,†] Zhonghua Sun,[†] Yaoming Xie,[‡] R. Bruce King,*[,‡] and Henry F. Schaefer, III[‡]

[†]School of Physical Science and Technology, Southwest Jiaotong University, Chengdu 610031, P. R. China

[‡]Department of Chemistry and Center for Computational Chemistry, University of Georgia, Athens, Georgia 30602, United States

Supporting Information

ABSTRACT: The trinuclear derivative $Fe_3(C_8H_8)_3$ was synthesized in 2009 by Lavallo and Grubbs via the reaction of $Fe(C_8H_8)_2$ with a bulky heterocyclic carbene. This fascinating structure is the first example of a derivative of the well-known $Fe_3(CO)_{12}$ in which all 12 carbonyl groups have been replaced by hydrocarbon ligands. The density functional theory predicts a structure having a central Fe_3 equilateral triangle with ∼2.9 Å Fe−Fe single bonded edges bridged by η^5,η^3-C_8H_8 ligands. This structure is close to the experimental structure, determined by X-ray crystallography. The related hypoelectronic $M_3(C_8H_8)_3$ derivatives (M = Cr, V, Ti) are predicted to have central scalene M_3 triangles with edge lengths and Wiberg bond indices (WBIs) corresponding to one formal single M−M bond, one formal double M═M bond, and one formal triple M≡M bond. For $Mn_3(C_8H_8)_3$, both a doublet structure with one Mn═Mn double bond and two Mn−Mn single bonds in the Mn_3 triangle, and a quartet structure with two Mn═Mn double bonds and one Mn−Mn single bond are predicted. The hyperelectronic derivatives $M_3(C_8H_8)_3$ have weaker direct M−M interactions in their M_3 triangles, as indicated by both the M−M distances and the WBIs. Thus, $Ni_3(C_8H_8)_3$ has bis(trihapto) η^3,η^3-C_8H_8 ligands bridging the edges of a central approximately equilateral Ni_3 triangle with long Ni···Ni distances of ∼3.7 Å. The WBIs indicate very little direct Ni−Ni bonding in this Ni_3 triangle and thus a local nickel environment in the singlet $Ni_3(C_8H_8)_3$ similar to that observed for diallylnickel $(\eta^3\text{-}C_3H_5)_2Ni$.

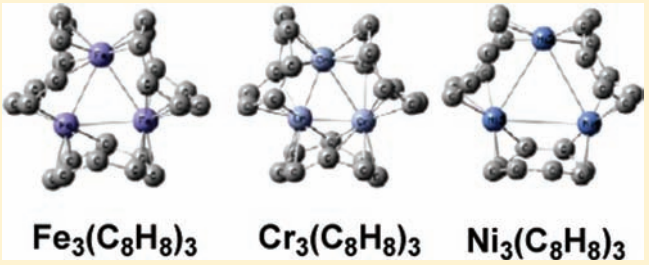

1. INTRODUCTION

The chemistry of trinuclear transition metal derivatives containing central metal triangles dates back to the discovery of $Fe_3(CO)_{12}$. What we now know to be $Fe_3(CO)_{12}$ is the green−black solid iron tetracarbonyl first prepared by Dewar and Jones in 1907.[1] The formulation of this material as the trimer $Fe_3(CO)_{12}$ was first demonstrated by Hieber and Becker[2,3] using a cryoscopic molecular weight determination in $Fe(CO)_5$. Subsequent elucidation of the nature of the metal−metal bonding and the arrangement of the 12 carbonyl groups in $Fe_3(CO)_{12}$ using X-ray crystallography followed a tortuous route[4] owing to disorder problems. Finally, in 1966 Wei and Dahl[5] determined definitively the correct C_{2v} doubly bridged isosceles triangular structure $Fe_3(CO)_{10}(\mu\text{-}CO)_2$ (Figure 1). Subsequently, Cotton and Troup[6] found more precise geometrical parameters for $Fe_3(CO)_{10}(\mu\text{-}CO)_2$. In contrast to the doubly bridged triiron dodecacarbonyl structure, the ruthenium and osmium analogues $M_3(CO)_{12}$ (M = Ru,[7] Os[8,9]) were shown to have D_{3h} unbridged structures with M_3 equilateral triangles (Figure 1).

A question of interest is whether all 12 carbonyl groups in $Fe_3(CO)_{12}$ can be replaced by hydrocarbon ligands. This has never been achieved by a direct reaction of $Fe_3(CO)_{12}$ with any hydrocarbon ligand since conditions forceful enough to replace all 12 carbonyl groups appear to rupture the central Fe_3 triangle. However, Lavallo and Grubbs[10,11] recently reported the unusual reaction between the mononuclear cyclooctatetraene sandwich compound $Fe(\eta^6\text{-}C_8H_8)(\eta^4\text{-}C_8H_8)$ and the bulky *N*-heterocyclic carbene $C_2H_4(NDipp)_2C$ (Dipp = 2,6-diisopropylphenyl) to give the trinuclear derivative $Fe_3(C_8H_8)_3$ (Figure 2). The stoichiometry of the $Fe_3(C_8H_8)_3$ product suggests a substitution product of $Fe_3(CO)_{12}$ in which the 12 C═C double bonds of three cyclooctatetraene units have replaced the 12 carbonyl groups. The structure of $Fe_3(C_8H_8)_3$, as determined by X-ray crystallography, has a central essentially equilateral Fe_3 triangle with an edge length of ∼2.82 Å. The three cyclooctatetraene ligands bridge the three Fe−Fe bonds but as pentahapto-trihapto η^5,η^3-C_8H_8 ligands rather than bis(tetrahapto) η^4,η^4-C_8H_8 ligands. In this $Fe_3(C_8H_8)_3$ structure, the iron atoms have the favored 18-electron configuration, just as they do in $Fe_3(CO)_{12}$.

The existence of $Fe_3(C_8H_8)_3$ having an equilateral Fe_3 triangle of Fe−Fe single bonds raises the question of the preferred

Received: February 17, 2011
Published: September 06, 2011

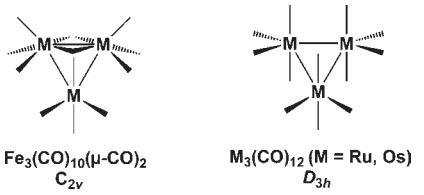

Figure 1. Comparison of the C_{2v} doubly bridged $Fe_3(CO)_{10}(\mu\text{-}CO)_2$ structure for $Fe_3(CO)_{12}$ with the D_{3h} unbridged $M_3(CO)_{12}$ (M = Ru, Os) structures. Carbonyl groups are omitted for clarity.

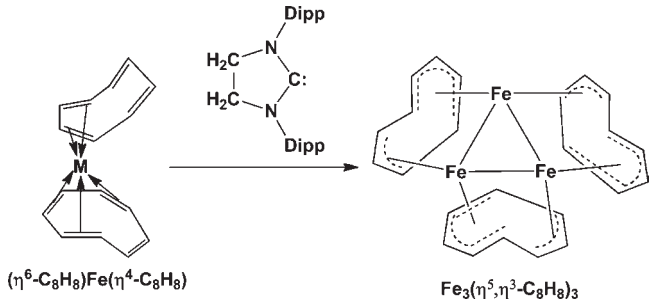

Figure 2. Conversion of the mononuclear $Fe(\eta^6\text{-}C_8H_8)(\eta^4\text{-}C_8H_8)$ to the trinuclear $Fe_3(\eta^5,\eta^3\text{-}C_8H_8)_3$ using an *N*-heterocyclic carbene catalyst.

structures for the other $M_3(C_8H_8)_3$ derivatives of the first row transition metals. The 18-electron rule suggests that the metals before Fe in the periodic table, namely, Mn, Cr, V, and Ti, should form $M_3(C_8H_8)_3$ derivatives with fully bonded C_8H_8 rings using all eight carbon atoms and multiple bonding within the M_3 triangle. Such derivatives can be considered as hypoelectronic derivatives relative to $Fe_3(C_8H_8)_3$. Conversely, $Co_3(C_8H_8)_3$ and $Ni_3(C_8H_8)_3$ would be expected to have structures with partially bonded C_8H_8 rings containing uncomplexed C═C double bonds and/or nonbonding edges in the M_3 triangle. Such derivatives can be considered as hyperelectronic derivatives, again relative to $Fe_3(C_8H_8)_3$. We now report our theoretical studies on the preferred structures and geometries for these $M_3(C_8H_8)_3$ derivatives (M = Ti, V, Cr, Mn, Fe, Co, and Ni).

2. COMPUTATIONAL METHODS

Electron correlation effects were included by employing density functional theory (DFT) methods, which have evolved as a practical and effective computational tool, especially for organometallic compounds.[12−26] The reliability of such density functional theory (DFT) methods is governed by the effectiveness of the approximate exchange-correlation (XC) energy functional. We chose three DFT methods, namely, the B3LYP, BP86, and mPW1PW91 methods, which are constructed in very different ways. The B3LYP method is a hybrid HF/DFT method using a combination of the three-parameter Becke functional (B3)[27] with the Lee−Yang−Parr (LYP) generalized gradient correlation functional.[28] This method includes exact exchange and is calibrated by fitting three parameters to a set of experimental results. The BP86 method combines Becke's 1988 exchange functional (B)[29] with Perdew's 1986 gradient-corrected correlation functional (P86).[30] This method does not include exact exchange and is mainly deduced by forcing the functional to satisfy certain exact constraints based on first principles. The newer generation mPW1PW91 method combines the Perdew's 1991 gradient-corrected correlation functional[31] with the

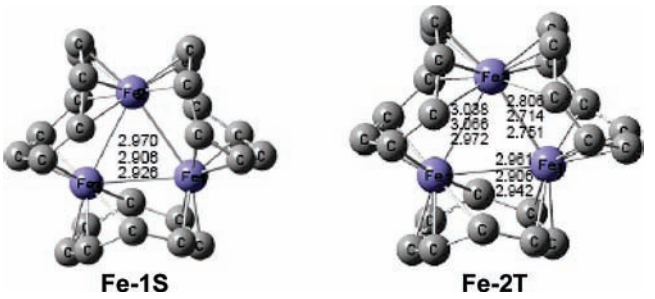

Figure 3. Optimized geometries for the $Fe_3(C_8H_8)_3$ structures. In Figures 3 to 9, the upper distances were determined by the B3LYP method, the middle distances by the BP86 method, and the lower distances by the mPW1PW91 method.

1996 exchange functional of Gill[32] and the Barone's modified PW91 exchange functional.[33] When these three very different DFT methods agree, reasonable predictions can be made. However, Reiher and collaborators[34] have found that B3LYP favors the high-spin state, and BP86 favors the low-spin state for a series of the Fe(II)-S complexes. In this work, a similar tendency for the B3LYP method and the mPW1PW91 method to favor higher spin states relative to the BP86 method was observed for the $M_3(C_8H_8)_3$ derivatives (M = Cr, Mn, Fe, and Co).

For carbon, the double-ζ plus polarization (DZP) basis set used here adds one set of pure spherical harmonic d functions with an orbital exponent $\alpha_d(C) = 0.75$ to the standard Huzinaga−Dunning contracted DZ sets[35,36] and is designated (9s5p1d/4s2p1d). For H, a set of p polarization functions $\alpha_p(H) = 0.75$ is added to the Huzinaga−Dunning DZ sets. For the first row transition metals, in our loosely contracted DZP basis set, the Wachters' primitive sets[37] are used but augmented by two sets of p functions and one set of d functions and contracted following Hood, Pitzer, and Schaefer,[38] and designated (14s11p6d/10s8p3d).

The geometries of all structures were fully optimized using the three DFT methods. The harmonic vibrational frequencies were determined at the same levels by evaluating analytically the second derivatives of the energy with respect to the nuclear coordinates. The corresponding infrared intensities were evaluated analytically as well. All of the computations were carried out with the Gaussian 09 program[39] in which the fine grid (75,302) is the default for evaluating integrals numerically. In some cases a finer (99,590) integration grid was used for the optimization to remove small imaginary vibrational frequencies.[40]

In the search for minima, low magnitude imaginary vibrational frequencies are suspect because the numerical integration procedures used in existing DFT methods have significant limitations.[41] Thus, an imaginary vibrational frequency of a magnitude less than 50i cm^{-1} should imply that there is a minimum with energy very similar to that of the stationary point in question. All of the final optimized structures reported in this Article have only real vibrational frequencies, unless otherwise indicated.

The geometries of the complexes $M_3(C_8H_8)_3$ (M = Ti, V, Cr, Mn, Fe, Co, and Ni) were optimized in the electronic singlet and triplet states for Ti, Cr, Fe, and Ni and doublet and quartet states for V, Mn, and Co. The equilibrium geometries of the energetically low lying species of $M_3(C_8H_8)_3$ are shown in Figures 3 to 9, with all metal−metal bond distances given in angstroms. In these figures, the upper distances were obtained by the B3LYP method, the middle distances were obtained by the BP86 method, and the lower distances were obtained by the mPW1PW91 method. The structures are designated as **M-aX**, where **M** is the symbol of the central metal atom, **a** orders the structures according to relative energies, and **X** designates the spin states, using **S**, **D**, **T**, and **Q** for singlets, doublets, triplets, and quartets, respectively.

dx.doi.org/10.1021/ic200337w |*Inorg. Chem.* 2011, 50, 9256–9265

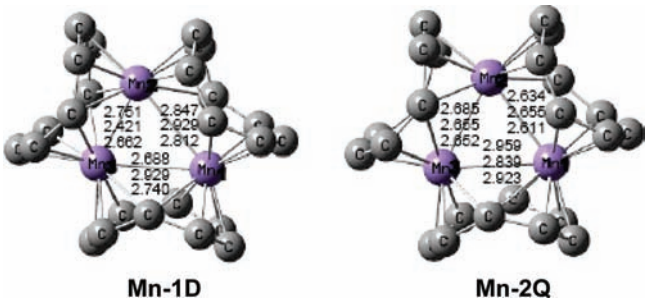

Figure 4. Optimized geometries for the $Mn_3(C_8H_8)_3$ structures.

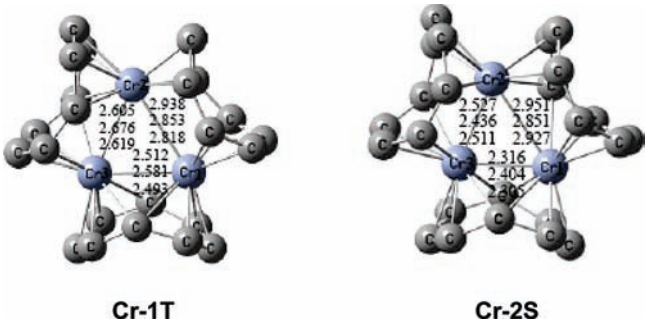

Figure 5. Optimized geometries for the $Cr_3(C_8H_8)_3$ structures.

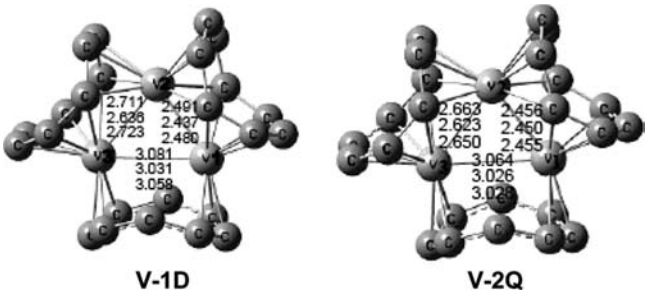

Figure 6. Optimized geometries for the $V_3(C_8H_8)_3$ structures.

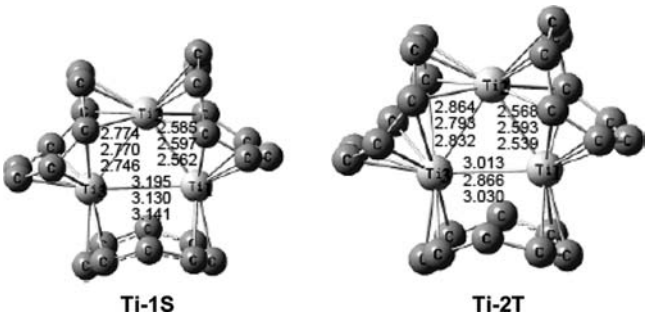

Figure 7. Optimized geometries for the $Ti_3(C_8H_8)_3$ structures.

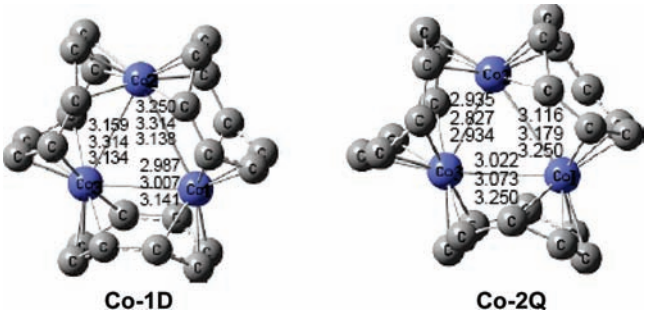

Figure 8. Optimized geometries for the $Co_3(C_8H_8)_3$ structures.

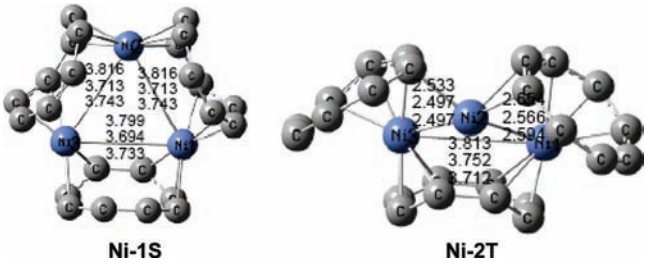

Figure 9. Optimized geometries for the $Ni_3(C_8H_8)_3$ structures.

3. RESULTS AND DISCUSSION

3.1. Iron Derivative $Fe_3(C_8H_8)_3$. The three iron atoms in the optimized singlet $Fe_3(C_8H_8)_3$ structure **Fe-1S** form a perfect equilateral triangle. Each of the three bridging COT ligands adopt η^5 and η^3 coordination modes, crowning the iron triangle to form a six-pointed star. This leads to the favored 18-electron configuration for each of the iron atoms (Figure 3 and Table 1). The angles centered at each Fe atom are 60°, and the Fe−Fe bond distances are 2.970 Å (B3LYP), 2.906 Å (BP86), and 2.926 Å (mPW1PW91). These BP86 distances are close to the known experimental structure[10] in which Fe1−Fe2 = 2.829 Å, Fe2−Fe3 = 2.830 Å, and Fe1−Fe3 = 2.815 Å. We find a related $Fe_3(C_8H_8)_3$ structure for the triplet **Fe-2T**. However, the Fe_3 triangle in **Fe-2T** is scalene rather than equilateral because of the Jahn−Teller effect.[42,43] Thus, the Fe−Fe bond distances in **Fe-2T** are 2.806/3.038/2.961 Å (B3LYP), 2.714/3.066/2.906 Å (BP86), or 2.751/2.972/2.942 Å (mPW1PW91). For **Fe-2T**, one tetrahapto ring and one trihapto C_8H_8 ring are found for the Fe1(COT) unit, one tetrahapto ring and one pentahapto C_8H_8 ring for the Fe2(COT) unit, and one pentahapto ring and one trihapto C_8H_8 ring for the Fe3(COT) unit, as indicated by the Fe−C bond distances. The singlet structure **Fe-1S** is predicted to lie 2.8 kcal/mol below the triplet structure **Fe-2T** by the BP86 method. However, the B3LYP and mPW1PW91 methods predict a lower energy for the triplet structure **Fe-2T**, namely, 8.1 or 9.8 kcal/mol below the singlet structure **Fe-1S**. The triplet structure **Fe-2T** has significant spin contamination by the B3LYP and mPW1PW91 methods as indicated by $\langle S^2 \rangle$ values of 2.29 and 2.40, respectively, relative to an ideal value of $S(S + 1) = 2$. Because of this spin contamination, the B3LYP and mPW1PW91 relative energy predictions for the singlet−triplet separation in $Fe_3(C_8H_8)_3$ should be considered as less reliable than that of the BP86 prediction. This is consistent with the experimental observation[10,11] of the singlet structure **Fe-1S** rather than the triplet state **Fe-2T** as the ground state of $Fe_3(C_8H_8)_3$.

3.2. Hypoelectronic Derivatives $M_3(C_8H_8)_3$ (M = Mn, Cr, V, and Ti). *3.2.1. $Mn_3(C_8H_8)_3$.* The energies of the doublet $Mn_3(C_8H_8)_3$ structure **Mn-1D** and the quartet structure **Mn-2Q** are very close (Figure 4 and Table 2). The B3LYP and mPW1PW91 methods predict **Mn-2Q** to lie 1.4 and 2.9 kcal/mol below

dx.doi.org/10.1021/ic200337w |*Inorg. Chem.* 2011, 50, 9256–9265

Table 1. Bond Distances (in Å), Total Energies (E in Hartree), Relative Energies (ΔE in kcal/mol), Imaginary Vibrational Frequencies, and Spin Expectation Values $\langle S^2\rangle$ for the $Fe_3(C_8H_8)_3$ Structures.[a]

	Fe-1S (C_{3h})				Fe-2T (C_s)		
	B3LYP	BP86	mPW1PW91		B3LYP	BP86	mPW1PW91
Fe1−(η^5-COT1)	2.143	2.139	2.113	Fe1−(η^4-COT1)	2.137	2.114	2.104
Fe1−(η^3-COT3)	2.058	2.047	2.036	Fe1−(η^3-COT3)	2.154	2.135	2.122
Fe2−(η^3-COT1)	2.058	2.047	2.036	Fe2−(η^4-COT1)	2.206	2.128	2.177
Fe2−(η^5-COT2)	2.143	2.139	2.113	Fe2−(η^5-COT2)	2.144	2.088	2.136
Fe3−(η^3-COT2)	2.058	2.047	2.036	Fe3−(η^3-COT2)	2.120	2.169	2.090
Fe3−(η^5-COT3)	2.143	2.139	2.113	Fe3−(η^5-COT3)	2.070	2.063	2.048
Fe1−Fe2	2.970	2.906	2.926	Fe1−Fe2	2.806	2.714	2.751
Fe2−Fe3	2.970	2.906	2.926	Fe2−Fe3	3.038	3.066	2.972
Fe3−Fe1	2.970	2.906	2.926	Fe3−Fe1	2.961	2.906	2.942
− energy	4720.19989	4720.88926	4720.20283	− energy	4720.21283	4720.88500	4720.21840
ΔE	0.0	0.0	0.0	ΔE	−8.1	2.8	−9.8
imaginary frequencies	39i	none	none	imaginary frequencies	none	none	none
$\langle S^2\rangle$	0.00	0.00	0.00	$\langle S^2\rangle$	2.29	2.10	2.40

[a] In Tables 1 to 8, the labels of the metal atoms and the C_8H_8-rings are indicated by 1, 2, 3 counterclockwise from the right. Average M-C_8H_8 ring bond distances shown.

Table 2. Bond Distances (in Å), Total Energies (E in Hartree), Relative Energies (ΔE in kcal/mol), Imaginary Vibrational Frequencies (cm^{-1}), and Spin Expectation Values $\langle S^2\rangle$ for the $Mn_3(C_8H_8)_3$ Structures

	Mn-1D				Mn-2Q		
	B3LYP (C_1)	BP86 (C_2)	mPW1PW91 (C_1)		B3LYP (C_1)	BP86 (C_2)	mPW1PW91 (C_1)
Mn1−(η^4-COT1)	2.188	2.190	2.150	Mn1−(η^4-COT1)	2.197	2.194	2.170
Mn1−(η^5-COT3)	2.209	2.162	2.172	Mn1−(η^5-COT3)	2.260	2.149	2.212
Mn2−(η^5-COT1)	2.193	2.165	2.427	Mn2−(η^4-COT1)	2.220	2.260	2.190
Mn2−(η^5-COT2)	2.200	2.165	2.183	Mn2−(η^4-COT2)	2.220	2.260	2.165
Mn3−(η^4-COT2)	2.246	2.190	2.210	Mn3−(η^4-COT2)	2.278	2.194	2.145
Mn3−(η^5-COT3)	2.167	2.162	2.135	Mn3−(η^5-COT3)	2.241	2.230	2.095
Mn1−Mn2	2.847	2.929	2.812	Mn1−Mn2	2.634	2.655	2.611
Mn2−Mn3	2.688	2.929	2.740	Mn2−Mn3	2.685	2.655	2.652
Mn3−Mn1	2.751	2.421	2.662	Mn3−Mn1	2.959	2.839	2.923
− energy	4382.02512	4382.64893	4382.01294	− energy	4382.02740	4382.64275	4382.01756
ΔE	0.0	0.0	0.0	ΔE	−1.4	3.9	−2.9
imaginary frequencies	none	none	none	imaginary frequencies	none	none	none
$\langle S^2\rangle$	1.22	0.77	1.35	$\langle S^2\rangle$	4.11	3.86	4.22

Mn-1D, respectively, whereas the BP86 method predicts **Mn-2Q** to lie 3.9 kcal/mol above **Mn-1D**. Significant spin contamination for both **Mn-1D** and **Mn-2Q** were found by the B3LYP and mPW1PW91 methods as indicated by the $\langle S^2\rangle$ values of 1.22/1.35 and 4.11/4.22 versus ideal values of 0.75 and 3.75, respectively. For this reason, the BP86 results may be considered to be more reliable than the B3LYP and mPW1PW91 results.

The Mn1(COT) and Mn3(COT) units in each $Mn_3(C_8H_8)_3$ structure have one pentahapto C_8H_8 ring and one tetrahapto C_8H_8 ring in both the doublet and quartet $Mn_3(C_8H_8)_3$ structures, **Mn-1D** and **Mn-2Q**, as indicated by the Mn−C distances. However, the Mn2(COT) unit has two pentahapto C_8H_8 rings in the doublet $Mn_3(C_8H_8)_3$ structure **Mn-1D** and two tetrahapto C_8H_8 rings in the quartet $Mn_3(C_8H_8)_3$ structure **Mn-2Q**. Both the doublet **Mn-1D** (BP86) and the quartet **Mn-2Q** (BP86) have C_2 symmetry with isosceles Mn_3 triangles. The two equal edges of the Mn_3 isosceles triangle are predicted to be 2.929 Å in **Mn-1D** and 2.655 Å in **Mn-2Q** by the BP86 method. In the **Mn-1D** structure, the remaining Mn−Mn distance of 2.421 Å is much shorter suggesting a formal double or triple bond.

3.2.2. $Cr_3(C_8H_8)_3$. The triplet electronic state $Cr_3(C_8H_8)_3$ structure **Cr-1T** (Figure 5 and Table 3) is predicted to be the global minimum. The singlet $Cr_3(C_8H_8)_3$ structure **Cr-2S** lies 8.5 kcal/mol (B3LYP), 6.0 kcal/mol (BP86), or 3.4 kcal/mol (mPW1PW91) in energy above the triplet structure **Cr-1T**. The Cr−C distances in each structure indicate one pentahapto C_8H_8 ring and one tetrahapto C_8H_8 ring for each Cr(COT) unit. The Cr−Cr bond distances in the singlet **Cr-2S** are Cr1−Cr2 = 2.951 Å (B3LYP), 2.851 Å (BP86), or 2.927 Å (mPW1PW91), Cr2═Cr3 = 2.527 Å (B3LYP), 2.436 Å (BP86), or 2.511 Å (mPW1PW91), and Cr1≡Cr3 = 2.316 Å (B3LYP), 2.404 Å (BP86), or 2.305 Å (mPW1PW91). This corresponds to formal single, double, and

dx.doi.org/10.1021/ic200337w |*Inorg. Chem.* 2011, 50, 9256–9265

Table 3. Bond Distances (in Å), Total Energies (E in Hartree), Relative Energies (ΔE in kcal/mol), Imaginary Vibrational Frequencies, and Spin Expectation Values $\langle S^2\rangle$ for the $Cr_3(C_8H_8)_3$ Structures

	Cr-2S			Cr-1T		
	B3LYP (C_1)	BP86 (C_1)	mPW1PW91	B3LYP(C_s)	BP86 (C_s)	mPW1PW91
Cr1−(η^4-COT1)	2.352	2.259	2.302	2.277	2.206	2.211
Cr1−(η^5-COT3)	2.190	2.196	2.161	2.236	2.221	2.280
Cr2−(η^4-COT1)	2.311	2.223	2.156	2.310	2.199	2.167
Cr2−(η^5-COT2)	2.236	2.203	2.237	2.255	2.212	2.219
Cr3−(η^4-COT2)	2.259	2.227	2.217	2.242	2.200	2.198
Cr3−(η^5-COT3)	2.190	2.208	2.158	2.284	2.226	2.215
Cr1−Cr2	2.951	2.851	2.927	2.938	2.853	2.818
Cr2−Cr3	2.527	2.436	2.511	2.605	2.676	2.619
Cr3−Cr1	2.316	2.404	2.305	2.512	2.581	2.493
− energy	4062.45804	4063.02313	4062.42575	4062.47165	4063.03532	4062.43118
ΔE	8.5	6.0	3.4	0.0	0.0	0.0
imaginary frequencies	none	none	none	45i	none	29i
$\langle S^2\rangle$	0.00	0.00	0.00	2.47	2.04	3.07

Table 4. Bond Distances (in Å), Total Energies (E in Hartree), Relative Energies (ΔE in kcal/mol), and Spin Expectation Values $\langle S^2\rangle$ for the $V_3(C_8H_8)_3$ Structures

	V-1D (C_s)			V-2Q (C_s)		
	B3LYP	BP86	mPW1PW91	B3LYP	BP86	mPW1PW91
V1−(η^5-COT1)	2.745	2.725	2.246	2.256	2.249	2.233
V1−(η^3-COT3)	2.907	2.856	2.268	2.289	2.259	2.261
V2−(η^5-COT1)	2.724	2.695	2.234	2.248	2.240	2.219
V2−(η^4-COT2)	3.069	3.042	2.290	2.299	2.285	2.264
V3−(η^6-COT2)	2.553	2.527	2.270	2.296	2.285	2.267
V3−(η^3-COT3)	2.995	2.990	2.220	2.257	2.242	2.227
V1−V2	2.491	2.437	2.480	2.458	2.450	2.455
V2−V3	2.711	2.636	2.723	2.663	2.623	2.650
V3−V1	3.081	3.031	3.058	3.064	3.026	3.028
− energy	3761.16410	3761.61626	3761.11960	3761.15099	3761.61102	3761.10851
ΔE	0.0	0.0	0.0	8.2	3.3	7.0
$\langle S^2\rangle$	2.49	1.86	2.57	4.01	3.79	4.15

triple bonds, respectively, for the B3LYP and mPW1PW91 results. Such bond assignments give each chromium atom in **Cr-2S** the expected 18-electron configuration for a singlet, assuming a formal positive charge on the chromium atom connected to a double bond and a triple bond, i.e., Cr3, and a formal negative charge on the chromium atom connected to a single bond and a double bond, i.e., Cr2. However, the Cr−Cr distances in the BP86 singlet structure **Cr-2S** are more difficult to interpret since the two shortest Cr−Cr distances are nearly equal at 2.42 ± 0.02 Å. This suggests one single bond and two Cr−Cr bonds of orders between two and three in the Cr_3 triangle of **Cr-2S**, which makes **Cr-2S** isosceles rather than scalene. For this reason, a singlet $Cr_3(C_8H_8)_3$ structure with a Cr_3 isosceles triangle was used as a starting structure for reoptimization constraining the symmetry to C_2, i.e., forcing the Cr_3 triangle to remain isosceles. However, the resulting singlet structures with a Cr_3 isosceles triangle were found to have a significant imaginary vibrational frequency. Following the corresponding normal mode led to the structure **Cr-2S** (Figure 5) with a scalene Cr_3 triangle. The Cr2−Cr3 and Cr1−Cr3 distances in **Cr-1T** are shorter than the corresponding Cr−Cr distances in **Cr-2S** (B3LYP). However, there is significant spin contamination in the triplet $Cr_3(C_8H_8)_3$ structure **Cr-1T** by the B3LYP and mPW1PW91 methods, i.e., $\langle S^2\rangle$ = 2.47 (B3LYP) or 3.07 (mPW1PW91) versus an ideal value of 2.

3.2.3. $V_3(C_8H_8)_3$. The optimized structures **V-1D** and **V-2Q** for the doublet and quartet spin states of $V_3(C_8H_8)_3$ are very similar (Figure 6 and Table 4). The V_3 triangles are scalene triangles with V1−V3 distances of 3.05 ± 0.03 Å, V2═V3 distances of 2.68 ± 0.04 Å, and V1≡V2 distances of 2.47 ± 0.02 Å, corresponding to formal single, double, and triple bonds, respectively. The quartet $V_3(C_8H_8)_3$ structure **V-2Q** lies 8.2 kcal/mol (B3LYP), 3.3 kcal/mol (BP86), or 7.0 kcal/mol (mPW1PW91) above **V-1D**. However, there is significant spin contamination in both the doublet and quartet $V_3(C_8H_8)_3$ structures as indicated by the $\langle S^2\rangle$ values considerably above the ideal $\langle S^2\rangle$ values of 0.75 and 3.75 for doublets and quartets, respectively.

3.2.4. $Ti_3(C_8H_8)_3$. The singlet structure **Ti-1S** and the triplet structure **Ti-2T** are found for $Ti_3(C_8H_8)_3$ (Figure 7 and Table 5).

dx.doi.org/10.1021/ic200337w |*Inorg. Chem.* 2011, 50, 9256–9265

Table 5. Bond Distances (in Å), Total Energies (E in Hartree), Relative Energies (ΔE in kcal/mol), and Spin Expectation Values $\langle S^2 \rangle$ for the $Ti_3(C_8H_8)_3$ Structures[a]

	Ti-1S (C_s)			Ti-2T (C_s)		
	B3LYP	BP86	mPW1PW91	B3LYP	BP86	mPW1PW91
Ti1−(η^5-COT1)	2.313	2.315	2.288	2.357	2.360	2.331
Ti1−(η^3-COT3)	2.322	2.315	2.297	2.377	2.331	2.343
Ti2−(η^5-COT1)	2.305	2.313	2.280	2.326	2.334	2.297
Ti2−(η^4-COT2)	2.337	2.319	2.306	2.346	2.354	2.309
Ti3−(η^6-COT2)	2.316	2.327	2.289	2.399	2.456	2.239
Ti3−(η^3-COT3)	2.331	2.314	2.302	2.294	2.295	2.269
Ti1−Ti2	2.585	2.597	2.562	2.568	2.593	2.539
Ti2−Ti3	2.774	2.770	2.746	2.864	2.793	2.832
Ti3−Ti1	3.195	3.130	3.141	3.013	2.866	3.030
− energy	3477.55738	3477.93648	3477.48920	3477.54654	3477.92632	3477.48124
ΔE	0.0	0.0	0.0	6.8	6.4	5.0
$\langle S^2 \rangle$	0.00	0.00	0.00	2.11	2.01	2.10

[a] Average M-C_8H_8 ring bond distance.

Table 6. Bond Distances (in Å), Total Energies (E in Hartree), Relative Energies (ΔE in kcal/mol), and Spin Expectation Values $\langle S^2 \rangle$ for the $Co_3(C_8H_8)_3$ Structures[a]

	Co-1D			Co-2Q (C_1)		
	B3LYP (C_1)	BP86 (C_2)	mPW1PW91 (C_1)	B3LYP	BP86	mPW1PW91
Co1−(η^3-COT1)	2.165	2.084	2.063	2.241	2.094	2.234
Co1−(η^5-COT3)	2.295	2.084	2.139	2.275	2.159	2.234
Co2−(η^4-COT1)	2.151	2.096	2.149	2.107	2.135	2.146
Co2−(η^3-COT2)	2.075	2.119	2.063	2.047	2.063	2.204
Co3−(η^5-COT2)	2.188	2.119	2.135	2.206	2.163	2.204
Co3−(η^3-COT3)	2.093	2.096	2.070	2.102	2.073	2.146
Co1−Co2	3.250	3.314	3.138	3.116	3.179	3.250
Co2−Co3	2.987	3.314	3.134	2.935	2.827	2.934
Co3−Co1	3.159	3.007	3.141	3.022	3.073	3.250
− energy	5077.41239	5078.11905	5077.43881	5077.40721	5078.10228	5077.42804
ΔE	0.0	0.00	0.00	3.3	10.5	6.8
$\langle S^2 \rangle$	2.22	0.77	2.11	4.02	3.82	4.31

[a] Average M-C_8H_8 ring bond distance.

These structures are genuine minima without any imaginary vibrational frequencies. The global minimum is the singlet **Ti-1S**, which lies 6.8 kcal/mol (B3LYP), 6.4 kcal/mol (BP86), or 5.0 kcal/mol (mPW1PW91) below the triplet **Ti-2T**. The Ti−C distances indicate that one pentahapto and one trihapto C_8H_8 ring are found in the Ti1(COT) unit, one pentahapto and one tetrahapto C_8H_8 ring in the Ti2(COT) unit, and one hexahapto and one trihapto C_8H_8 ring in the Ti3(COT) unit. The Ti_3 triangle in **Ti-1S** is a scalene triangle with a Ti1−Ti3 single bond distance of 3.195 Å (B3LYP) or 3.130 Å (BP86), a Ti2═Ti3 double bond distance of 2.774 Å (B3LYP) or 2.770 Å (BP86), and a Ti1≡Ti2 triple bond distance of 2.585 Å (B3LYP) or 2.597 Å (BP86). The Ti_3 triangle in **Ti-1S** is a scalene triangle with a Ti1−Ti3 single bond distance of 3.195 Å (B3LYP), 3.130 Å (BP86), or 3.141 Å (mPW1PW91), a Ti2═Ti3 double bond distance of 2.774 Å (B3LYP), 2.770 Å (BP86), or 2.746 Å (mPW1PW91), and a Ti1≡Ti2 triple bond distance of 2.585 Å (B3LYP), 2.597 Å (BP86), or 2.562 Å (mPW1PW91).Thus, the singlet **Ti-1S** structure has 16-electron configurations for all three titanium atoms, similar to that of the central titanium atom in the known complex[44,45] (η^8-C_8H_8)Ti(η^4-C_8H_8).

3.3. Hyperelectronic Derivatives $M_3(C_8H_8)_3$ (M = Co, Ni).

3.3.1. $Co_3(C_8H_8)_3$. Now, we move to systems in which electrons are added to $Fe_3(C_8H_8)_3$. The doublet structure **Co-1D** and the quartet structure **Co-2Q** for $Co_3(C_8H_8)_3$ are both true minima with no imaginary vibrational frequencies (Figure 8 and Table 6). The quartet structure **Co-2Q** lies 3.3 kcal/mol (B3LYP), 10.5 kcal/mol (BP86), or 6.8 kcal/mol (mPW1PW91) above the doublet structure **Co-1D**. Both structures have one trihapto C_8H_8 ring and one pentahapto C_8H_8 ring for the Co1(COT) and Co3(COT) units. The Co_3 triangle in the doublet structure **Co-1D** is an isosceles triangle by BP86. However, the Co_3 triangle in the quartet structure **Co-2Q** is clearly scalene rather than equilateral or isosceles. The relatively long Co−Co distances in the range of 2.83 to 3.32 Å suggest weak direct cobalt−cobalt interactions.

dx.doi.org/10.1021/ic200337w |*Inorg. Chem.* 2011, 50, 9256–9265

Table 7. Bond Distances (in Å), Total Energies (E in Hartree), Relative Energies (ΔE in kcal/mol), Imaginary Vibrational Frequencies, and Spin Expectation Values $\langle S^2 \rangle$ for the $Ni_3(C_8H_8)_3$ Structures[a]

	Ni-1S (C_s)				Ni-2T (C_1)		
	B3LYP	BP86	MPW1PW91		B3LYP	BP86	MPW1PW91
Ni1−(η^3-COT1)	2.071	2.064	2.043	Ni1−(η^3-COT1)	2.150	2.084	2.130
Ni1−(η^3-COT3)	2.071	2.064	2.043	Ni1−(η^4-COT3)	2.229	2.149	2.128
Ni2−(η^3-COT1)	2.071	2.066	2.042	Ni2−(η^2-COT1)	2.099	2.247	2.121
Ni2−(η^3-COT2)	2.071	2.066	2.042	Ni2−(η^2-COT2)	2.099	2.247	2.224
Ni3−(η^3-COT2)	2.071	2.064	2.042	Ni3-(η^3-COT2)	2.150	2.084	2.049
Ni3−(η^3-COT3)	2.071	2.064	2.042	Ni3−(η^4-COT3)	2.229	2.149	2.069
Ni1−Ni2	3.816	3.713	3.743	Ni1−Ni2	2.654	2.566	2.594
Ni2−Ni3	3.816	3.713	3.743	Ni2−Ni3	2.533	2.497	2.497
Ni3−Ni1	3.799	3.694	3.733	Ni3−Ni1	3.813	3.752	3.712
− energy	5454.072134	5454.79020	5454.09443	− energy	5454.05876	5454.77982	5454.08472
ΔE	0.0	0.0	0.0	ΔE	8.4	6.5	6.1
$\langle S^2 \rangle$	0.00	0.00	0.00	$\langle S^2 \rangle$	2.09	2.01	2.19

[a] Average M-C_8H_8 ring bond distance.

3.3.2. $Ni_3(C_8H_8)_3$. The global minimum $Ni_3(C_8H_8)_3$ structure is the C_s singlet **Ni-1S** in which all three C_8H_8 rings are bis(trihapto) ligands, and the Ni_3 triangle is approximately equilateral (Figure 9 and Table 7). The Ni···Ni distances are longer than 3.7 Å, clearly indicating the absence of direct nickel−nickel bonds between any of the pairs of nickel atoms. The triplet $Ni_3(C_8H_8)_3$ structure **Ni-2T** lies 8.4 kcal/mol (B3LYP), 6.5 kcal/mol (BP86), or 6.1 kcal/mol (mPW1PW91) above the singlet structure **Ni-1S**. The structure **Ni-2T** has one trihapto C_8H_8 ring and one tetrahapto C_8H_8 ring for the Ni1(COT) and Ni3(COT) units and one dihapto C_8H_8 ring for the Ni2(COT) unit. All of the Ni−Ni bond distances in the triplet structure **Ni-2T** are shorter than those in the singlet structure **Ni-1S** by the BP86 and mPW1PW91 methods.

3.4. Metal−Metal Bonding in the M_3 Triangles of the $M_3(C_8H_8)_3$ Derivatives. In order to gain additional insight into the metal−metal bonding in the M_3 triangles of the $M_3(C_8H_8)_3$ derivatives beyond that inferred from metal−metal bond lengths and electron counting, the Wiberg Bond Indices (WBIs) were determined by Natural Bond Orbital (NBO) analysis (Table 8).[46] The WBIs for the three equivalent Fe−Fe bonds in the experimentally known[10] singlet $Fe_3(C_8H_8)_3$ structure **Fe-1S** (Figure 3) are 0.22. This compares with the WBI of 0.18 found for the Fe−Fe bonds in the singlet unbridged D_{3h} isomer of $Fe_3(CO)_{12}$ in a previous theoretical study.[47] Thus, the WBI of the Fe−Fe bonds in **Fe-1S** indicates that they are single bonds as suggested above and are consistent with the 18-electron rule.

The hypoelectronic derivatives $M_3(C_8H_8)_3$ (M = Mn, Cr, V, and Ti) are suggested by the 18-electron rule and their M−M distances to have some metal−metal multiple bonding in their M_3 triangles. In many of the hypoelectronic $M_3(C_8H_8)_3$ structures with scalene M_3 triangles (M = Cr, V, and Ti), the WBIs support the pattern of one M−M single bond, one M═M double bond, and one M≡M triple bond but with wide ranges of WBIs, namely, from 0.24 to 0.45 for single bonds, 0.45 to 0.60 for double bonds, and 0.61 to 1.13 for triple bonds (Figure 10). These wide ranges of WBIs for a given formal metal−metal bond order in the $M_3(C_8H_8)_3$ derivatives are not surprising in view of the wide ranges of spin multiplicities and metal-electronic configurations in these complexes. Most significantly, a scalene M_3 triangle with one M−M single bond, one M═M double bond, and one M≡M triple bond is more favorable than an equilateral triangle with three M═M bonds (Figure 10). With a formal positive charge on the metal atom with one double and one triple bond to other metal atoms, a formal negative charge on the metal atom adjacent to one single and one double bond, and no formal charge on the third metal atom, the chromium atoms in $Cr_3(C_8H_8)_3$ (e.g., **Cr-2S** in Figure 5) have 18-electron configurations. Analogously, the vanadium atoms in $V_3(C_8H_8)_3$ (e.g., **V-1D** in Figure 6) have 17-electron configurations, and the titanium atoms in $Ti_3(C_8H_8)_3$ (e.g., **Ti-1S** in Figure 7) have 16-electron configurations.

These same electronic configurations are found in other types of known stable compounds of these early transition metals, e.g., the sandwich compounds (η^5-C_5H_5)M(η^7-C_7H_7) (M = Ti,[48] V,[49,50] and Cr[51−53]). Furthermore, a scalene triangle with one M−M single bond, one M═M double bond, and one M≡M triple bond in preference to an equilateral triangle with three M═M double bonds was previously predicted[47] for the unsaturated trinuclear iron carbonyl $Fe_3(CO)_9$. The instability of two M═M double bonds relative to one M−M single bond and one M≡M triple bond has previously been observed experimentally and predicted theoretically in the facile disproportionation of the Cr═Cr doubly bonded derivative (η^5-$C_5H_5)_2Cr_2(CO)_5$ at ambient conditions into the stable Cr−Cr singly bonded derivative (η^5-$C_5H_5)_2Cr_2(CO)_6$ plus the stable Cr≡Cr triply bonded derivative (η^5-$C_5H_5)_2Cr_2(CO)_4$.[54]

The B3LYP and BP86 methods do not agree well for the Mn_3 triangle in the doublet **Mn-1D**. However, the general patterns as well as the WBIs suggest two formal Mn−Mn single bonds and one Mn═Mn double bond, giving two of the three Mn atoms the favored 18-electron configuration and the third Mn atom a 17-electron configuration consistent with the doublet spin state. The Mn_3 triangle in the quartet **Mn-2Q** is clearly an isosceles triangle by the BP86 method. However, the edge-lengths and WBIs suggest two Mn═Mn double bonds and one Mn−Mn single bond.

The hyperelectronic $M_3(C_8H_8)_3$ derivatives (M = Co, Ni) do not require three formal metal−metal single bonds in their M_3 triangles to give each metal atom the favored 18-electron configuration if all three cyclooctatetraene ligands use all eight of

dx.doi.org/10.1021/ic200337w |*Inorg. Chem.* 2011, 50, 9256–9265

Table 8. Wiberg Bond Indices for the M−M bonds in the $M_3(C_8H_8)_3$ Structures (M = Ti, V, Cr, Mn, Fe, Co, and Ni)

		M−M Wiberg bond index			
complex		B3LYP	BP86	mPW1PW91	M−M formal bond order
Ti-1S	Ti (1)−Ti (2)	0.956	0.913	0.780	3
	Ti (2)−Ti (3)	0.567	0.604	0.467	2
	Ti (3)−Ti (1)	0.349	0.450	0.329	1
Ti-2T	Ti (1)−Ti (2)	0.717	0.847	0.101	3
	Ti (2)−Ti (3)	0.499	0.627	0.091	2
	Ti (3)−Ti (1)	0.402	0.631	0.064	1
V-1D	V(1)−V(2)	0.943	1.027	0.200	3
	V(2)−V(3)	0.463	0.595	0.199	2
	V(3)−V(1)	0.240	0.310	0.054	1
V-2Q	V(1)−V(2)	0.940	1.004	0.193	3
	V(2)−V(3)	0.524	0.598	0.111	2
	V(3)−V(1)	0.235	0.275	0.054	1
Cr-1S	Cr(1)−Cr(2)	0.307	0.486	0.186	1
	Cr(2)−Cr(3)	0.585	0.912	0.441	2 to 3
	Cr(3)−Cr(1)	1.127	0.951	0.882	3
Cr-2T	Cr(1)−Cr(2)	0.344	0.412	0.132	1
	Cr(2)−Cr(3)	0.450	0.598	0.142	2
	Cr(3)−Cr(1)	0.612	0.712	0.156	3
Mn-1D	Mn(1)−Mn(2)	0.296	0.292	0.058	1
	Mn(2)−Mn(3)	0.357	0.292	0.076	1
	Mn(3)−Mn(1)	0.381	0.754	0.080	2
Mn-2Q	Mn(1)−Mn(2)	0.381	0.426	0.133	1 to 2
	Mn(2)−Mn(3)	0.341	0.426	0.084	1 to 2
	Mn(3)−Mn(1)	0.229	0.314	0.051	1
Fe-1S	Fe(1)−Fe(2)	0.220	0.278	0.151	1
	Fe(2)−Fe(3)	0.220	0.278	0.151	1
	Fe(3)−Fe(1)	0.220	0.278	0.151	1
Fe-2T	Fe(1)−Fe(2)	0.221	0.243	0.036	1
	Fe(2)−Fe(3)	0.141	0.215	0.074	2
	Fe(3)−Fe(1)	0.202	0.220	0.036	1
Co-1D	Co(1)−Co(2)	0.089	0.140	0.055	1
	Co(2)−Co(3)	0.119	0.140	0.024	1
	Co(3)−Co(1)	0.095	0.197	0.023	1
Co-2Q	Co(1)−Co(2)	0.108	0.145	0.026	1
	Co(2)−Co(3)	0.140	0.177	0.029	1
	Co(3)−Co(1)	0.118	0.140	0.024	1
Ni-1S	Ni(1)−Ni(2)	0.032	0.061	0.022	0
	Ni(2)−Ni(3)	0.032	0.061	0.022	0
	Ni(3)−Ni(1)	0.032	0.062	0.022	0
Ni-2T	Ni(1)−Ni(2)	0.049	0.066	0.028	1
	Ni(2)−Ni(3)	0.049	0.060	0.028	1
	Ni(3)−Ni(1)	0.013	0.025	0.008	0

their carbon atoms to bond to the M_3 triangles. Their M−M distances are somewhat longer and the M−M bond WBIs are lower than those in the benchmark structure **Fe-1S** of the known[10] $Fe_3(C_8H_8)_3$. In the doublet and lowest energy $Co_3(C_8H_8)_3$ structure **Co-1D**, the Co−Co distances are ~3.2 ± 0.1 Å, and the WBIs are 0.10 ± 0.02 suggesting much weaker metal−metal bonding than the formal single bonds in the $Fe_3(C_8H_8)_3$ structure. The three Ni···Ni distances in the nearly equilateral Ni_3 triangle in the singlet $Ni_3(C_8H_8)_3$ structure **Ni-1S** (Figure 9) are clearly nonbonding distances of ~3.7 Å. The very weak Ni···Ni interactions along these edges are supported by very low WBIs of 0.04. The local nickel environments in **Ni-1S** can be considered to approach that of the nickel atom in the stable diallylnickel[55] $(\eta^3\text{-}C_3H_5)_2Ni$, particularly since the cyclooctatetraene ligands function as bis(trihapto) η^3,η^3-C_8H_8 ligands. The bis(trihapto) cyclooctatetraene ligands have one unusually short C═C distance of 1.369 Å (B3LYP) or 1.387 Å (BP86), which corresponds to the uncomplexed double bond.

3.5. Molecular Orbital Analyses. Analyses of the frontier molecular orbitals (MOs) (Figure 11) were performed for the

dx.doi.org/10.1021/ic200337w |*Inorg. Chem.* 2011, 50, 9256–9265

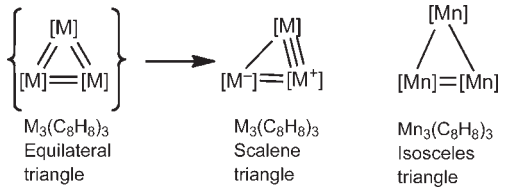

Figure 10. Types of M_3 triangles in hypoelectronic $M_3(C_8H_8)_3$ complexes.

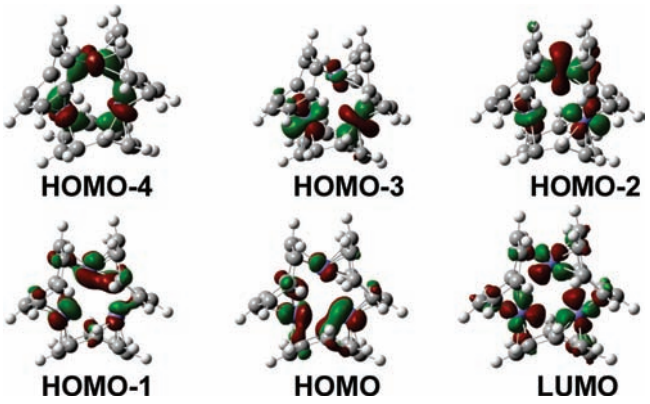

Figure 11. Frontier molecular orbitals of the $Fe_3(C_8H_8)_3$ complex **Fe-1S**.

Table 9. Fragmentation Energies (kcal/mol) for $M_3(C_8H_8)_3 \rightarrow 3M(C_8H_8)$

	B3LYP	BP86	mPW1PW91
$Ti_3(C_8H_8)_3$(**Ti-1S**) → $3Ti(C_8H_8)$	154.5	192.9	285.2
$V_3(C_8H_8)_3$(**V-1D**) → $3\,V(C_8H_8)$	202.9	249.1	275.4
$Cr_3(C_8H_8)_3$(**Cr-1T**) → $3Cr(C_8H_8)$	160.4	219.4	169.6
$Mn_3(C_8H_8)_3$(**Mn-1D**) → $3Mn(C_8H_8)$	187.6	260.0	199.5
$Fe_3(C_8H_8)_3$(**Fe-1S**) → $3Fe(C_8H_8)$	188.5	232.5	215.9
$Co_3(C_8H_8)_3$(**Co-1D**) → $3Co(C_8H_8)$	185.4	224.3	133.0
$Ni_3(C_8H_8)_3$(**Ni-1S**) → $3Ni(C_8H_8)$	90.7	107.2	103.6

lowest energy $Fe_3(C_8H_8)_3$ structures **Fe-1S** (Figure 3). These are seen to involve the metal d orbitals and thus relate primarily to the iron−iron interactions in the Fe_3 triangle.

3.6. Fragmentation Energies. The $M_3(C_8H_8)_3$ structures with the lowest spin multiplicities have the lowest energies except for $Cr_3(C_8H_8)_3$, where the triplet structure **Cr-1T** rather than the singlet structure **Cr-2S** (Figure 5) has the lowest energy. In order to calculate the fragmentation energies for $M_3(C_8H_8)_3 \rightarrow 3M(C_8H_8)$, the geometries of the $M(C_8H_8)$ fragments (M = Ti, V, Cr, Mn, Fe, Co, and Ni) were optimized. The lowest energy electronic states for the Ti, Fe, and Ni derivatives were found to be singlets, those for V, Mn, and Co were found to be doublets, and that for Cr was found to be a triplet. Furthermore, in the structures of the lowest energy $M(C_8H_8)$ fragments (M = Ti, V, Cr, Mn, and Co), the C_8H_8 rings are fully bonded as octahapto ligands. However, for the lowest energy $Fe(C_8H_8)$ and $Ni(C_8H_8)$ structures, a $\eta^{2,2}$-C_8H_8 tetrahapto ligand is found in which two nonadjacent C═C double bonds of the C_8H_8 ring are bonded to the metal atom. The optimized $M(C_8H_8)$ (M = Ti, V, Cr, Mn, and Co) structures and their energies are listed in the Supporting Information. Using these data, the energies for the fragmentation process $M_3(C_8H_8)_3 \rightarrow 3M(C_8H_8)$ are are all predicted to be very large ranging from 90 to 285 kcal/mol (Table 9).

Table 10. Reaction Energies (kcal/mol) for the Trimerization Reactions $3M(C_8H_8)_2 \rightarrow M_3(C_8H_8)_3 + 3(C_8H_8)$

	B3LYP	BP86	mPW1PW91
$3Ti(C_8H_8)_2 \rightarrow Ti_3(C_8H_8)_3 + 3(C_8H_8)$	63.5	73.6	65.1
$3V(C_8H_8)_2 \rightarrow V_3(C_8H_8)_3 + 3(C_8H_8)$	12.2	26.4	13.1
$3Cr(C_8H_8)_2 \rightarrow Cr_3(C_8H_8)_3 + 3(C_8H_8)$	29.2	4.9	39.6
$3Mn(C_8H_8)_2 \rightarrow Mn_3(C_8H_8)_3 + 3(C_8H_8)$	−9.9	−2.5	−7.2
$3Fe(C_8H_8)_2 \rightarrow Fe_3(C_8H_8)_3 + 3(C_8H_8)$	−14.9	5.4	−15.7
$3Co(C_8H_8)_2 \rightarrow Co_3(C_8H_8)_3 + 3(C_8H_8)$	−11.7	−17.5	−12.6
$3Ni(C_8H_8)_2 \rightarrow Ni_3(C_8H_8)_3 + 3(C_8H_8)$	−5.5	19.2	−5.3

Lavallo and Grubbs synthesized the trinuclear derivative $Fe_3(C_8H_8)_3$ by the reaction $3Fe(C_8H_8)_2 \rightarrow Fe_3(C_8H_8)_3 + 3(C_8H_8)$ using an *N*-heterocyclic carbene catalyst.[10,11] The $(C_8H_8)_2M$ derivatives of the first row transition metals were investigated in previous work using similar density functional theory methods.[56] The predicted energies for the trimerization reactions $3M(C_8H_8)_2 \rightarrow M_3(C_8H_8)_3 + 3(C_8H_8)$ using the previously calculated $M(C_8H_8)_2$ energies are listed in Table 10. The predicted reaction energies using the B3LYP and mPW1PW91 methods are in good agreement. These methods show the $3Fe(C_8H_8)_2 \rightarrow Fe_3(C_8H_8)_3 + 3(C_8H_8)$ reaction to be exothermic by ∼15 kcal/mol.

4. CONCLUSIONS

The iron atoms in the Lavallo−Grubbs[10] trinuclear complex $Fe_3(\eta^5,\eta^3\text{-}C_8H_8)_3$ are predicted to form an equilateral triangle with each ∼2.9 Å edge bridged by a pentahapto-trihapto cyclooctatetraene ligand, in agreement with the experimental structure. This structure may be regarded as a fully substituted hydrocarbon derivative of the well-known[1−6] $Fe_3(CO)_{12}$.

The hypoelectronic trinuclear $M_3(C_8H_8)_3$ derivatives relative to $Fe_3(C_8H_8)_3$, namely, those where M = Mn, Cr, V, and Ti, have structures with metal−metal distances and Wiberg Bond Indices suggesting multiple metal−metal bonding in their M_3 triangles. The M_3 triangles in $Cr_3(C_8H_8)_3$, $V_3(C_8H_8)_3$, and $Ti_3(C_8H_8)_3$ are scalene triangles with metal−metal distances and WBIs corresponding to one M−M single bond, M═M double bond, and M≡M triple bond. No isoelectronic structures with equilateral triangles of M═M double bonds were found for any of these $M_3(C_8H_8)_3$ structures. Both doublet and quartet structures are predicted for the manganese derivative $Mn_3(C_8H_8)_3$. The doublet structure appears to have one Mn═Mn double bond and two Mn−Mn single bonds in the Mn_3 triangle. The quartet $Mn_3(C_8H_8)_3$ structure also has an isosceles central Mn_3 triangle but with Mn−Mn distances suggesting two double bonds and one single bond.

The M_3 triangles in the hyperelectronic $M_3(C_8H_8)_3$ derivatives (M = Co, Ni) have longer M−M edges with smaller WBIs, indicating weaker direct M−M interactions. The nickel derivative $Ni_3(C_8H_8)_3$ has a singlet structure with an approximately equilateral Ni_3 triangle with ∼3.7 Å edges, which are too long for significant direct Ni−Ni bonding. The low WBIs of these Ni···Ni edges also indicate very weak Ni−Ni bonding. Since the cyclooctatetraene rings in this singlet $Ni_3(C_8H_8)_3$ structure

dx.doi.org/10.1021/ic200337w |*Inorg. Chem.* 2011, 50, 9256–9265

function as bis(trihapto) ligands, the local nickel environment may be considered to be similar to the known stable compound diallylnickel, $Ni(\eta^3\text{-}C_3H_5)_2$.

■ ASSOCIATED CONTENT

Supporting Information. Metal−carbon distances and carbon−carbon distance (in Å) for the $M_3(C_8H_8)_3$ (M = Ti, V, Cr, Mn, Fe, Co, Ni) structures (Tables S1 to S7); optimized coordinates for the $M_3(C_8H_8)_3$ (M = Ti, V, Cr, Mn, Fe, Co, Ni) structures; optimized structures and energies (Hartree) for C_8H_8 and $M(C_8H_8)$; complete Gaussian reference (ref 39). This material is available free of charge via the Internet at http://pubs.acs.org.

■ AUTHOR INFORMATION

Corresponding Authors

*E-mail: wanghyxx@yahoo.com (H.W.), rbking@chem.uga.edu (R.B.K.).

■ ACKNOWLEDGMENT

We are grateful to the China National Science Foundation (Grants 10774104 and 10974161), the Sichuan Province Youth Science and Technology Foundation (2008-20-360), and the U.S. National Science Foundation (Grants CHE-0716718 and CHE-1054286) for support of this work.

■ REFERENCES

(1) Dewar, J.; Jones, H. O. *Proc. R. Soc.* **1907**, *79A*, 66.
(2) Hieber, W.; Becker, E. *Chem. Ber.* **1930**, *63*, 1405.
(3) Hieber, W. *Z. Anorg. Allg. Chem.* **1932**, *203*, 165.
(4) See the historical article by Desiderato, R.; Dobson, G. R. *J. Chem. Educ.* **1982**, *59*, 752.
(5) Wei, C. H.; Dahl, L. F. *J. Am. Chem. Soc.* **1966**, *88*, 1821.
(6) Cotton, F. A.; Troup, J. M. *J. Am. Chem. Soc.* **1974**, *96*, 4155.
(7) Churchill, M. R.; Hollander, F. J.; Hutchinson, J. P. *Inorg. Chem.* **1977**, *16*, 2655.
(8) Corey, E. R.; Dahl, L. F. *Inorg. Chem.* **1962**, *1*, 521.
(9) Churchill, M. R.; DeBoer, B. G. *Inorg. Chem.* **1977**, *16*, 878.
(10) Lavallo, V.; Grubbs, R. H. *Science* **2009**, *326*, 559.
(11) Lavallo, V.; El-Batta, A.; Bertrand, G.; Grubbs, R. H. *Angew. Chem., Int. Ed.* **2011**, *50*, 268.
(12) Ehlers, A. W.; Frenking, G. *J. Am. Chem. Soc.* **1994**, *116*, 1514.
(13) Delley, B.; Wrinn, M.; Lüthi, H. P. *J. Chem. Phys.* **1994**, *100*, 5785.
(14) Li, J.; Schreckenbach, G.; Ziegler, T. *J. Am. Chem. Soc.* **1995**, *117*, 486.
(15) Jonas, V.; Thiel, W. *J. Chem. Phys.* **1995**, *102*, 8474.
(16) Barckholtz, T. A.; Bursten, B. E. *J. Am. Chem. Soc.* **1998**, *120*, 1926.
(17) Niu, S.; Hall, M. B. *Chem. Rev.* **2000**, *100*, 353.
(18) Macchi, P.; Sironi, A. *Coord. Chem. Rev.* **2003**, *238*, 383.
(19) Carreon, J.-L.; Harvey, J. N. *Phys. Chem. Chem. Phys.* **2006**, *8*, 93.
(20) Bühl, M.; Kabrede, H. *J. Chem. Theory Comput.* **2006**, *2*, 1282.
(21) Lundberg, M.; Siegbahn, P. E. M.; Morokuma, K. *Biochem.* **2008**, *47*, 1031.
(22) Sauriol, F.; Wong, E.; Leung, A. M. H.; Donaghue, I. E.; Baird, M. C.; Wondimagegn, T.; Ziegler, T. *Angew. Chem., Int. Ed.* **2009**, *48*, 3342.
(23) Harvey, J. N.; Jover, J.; Lloyd-Jones, G. C.; Mosely, J. D.; Murray, P.; Renny, J. S. *Angew. Chem., Int. Ed.* **2009**, *48*, 7612.
(24) Seiffert, N.; Bühl, M. *J. Am. Chem. Soc.* **2010**, *132*, 7605.
(25) Hull, J. F.; Balcells, D.; Sauer, E. L. O.; Raynaud, C.; Brudvig, G. W.; Crabtree, R. H.; Eisenstein, O. *J. Am. Chem. Soc.* **2010**, *132*, 7605.
(26) McNaughton, R. L.; Roemelt, M.; Chin, J. M.; Schrock, R. R.; Neese, F.; Hoffman, B. M. *J. Am. Chem. Soc.* **2010**, *132*, 8645.
(27) Becke, A. D. *J. Chem. Phys.* **1993**, *98*, 5648.
(28) Lee, C.; Yang, W.; Parr, R. G. *Phys. Rev. B* **1988**, *37*, 785.
(29) Becke, A. D. *Phys. Rev. A* **1988**, *38*, 3098.
(30) Perdew, J. P. *Phys. Rev. B* **1986**, *33*, 8822.
(31) Perdew, J. P. In *Electronic Structure of Solids*; Ziesche, P., Eschrig, H., Eds.; Akademie Verlag: Berlin, 1991; p 11.
(32) Gill, P. M. W. *Mol. Phys.* **1996**, *89*, 433.
(33) Adamo, C.; Barone, V. *J. Chem. Phys.* **1998**, *108*, 664.
(34) Reiher, M.; Salomon, O.; Hess, B. A. *Theor. Chem. Acc.* **2001**, *107*, 48.
(35) Dunning, T. H. *J. Chem. Phys.* **1970**, *53*, 2823.
(36) Huzinaga, S. *J. Chem. Phys.* **1965**, *42*, 1293.
(37) Wachters, A. J. H. *J. Chem. Phys.* **1970**, *52*, 1033.
(38) Hood, D. M.; Pitzer, R. M.; Schaefer, H. F. *J. Chem. Phys.* **1979**, *71*, 705.
(39) Frisch, M. J. et al. *Gaussian 09*, Revision A.02; Gaussian, Inc.: Wallingford, Connecticut, 2009.
(40) Papas, B. N.; Schaefer, H. F. *J. Mol. Struct.* **2006**, *768*, 175.
(41) Xie, Y.; Schaefer, H. F.; King, R. B. *J. Am. Chem. Soc.* **2000**, *122*, 8746.
(42) Eisfeld, W.; Viel, A. *J. Chem. Phys.* **2005**, *122*, 204317.
(43) Viel, A.; Eisfeld, W. *J. Chem. Phys.* **2004**, *120*, 4603.
(44) Breil, H.; Wilke, G. *Angew. Chem.* **1966**, *78*, 942.
(45) Dietrich, H.; Soltwisch, M. *Angew. Chem., Int. Ed.* **1969**, *8*, 765.
(46) Weinhold, F.; Landis, C. R. *Valency and Bonding: A Natural Bond Order Donor-Acceptor Perspective*; Cambridge University Press: Cambridge, U. K., 2005.
(47) Wang, H.; Xie, Y.; King, R. B.; Schaefer, H. F. *J. Am. Chem. Soc.* **2006**, *128*, 11376.
(48) Zeinstra, J. D.; de Boer, J. L. *J. Organomet. Chem.* **1973**, *54*, 207.
(49) King, R. B.; Stone, F. G. A. *J. Am. Chem. Soc.* **1959**, *81*, 5263.
(50) Engebretson, G.; Rundle, R. E. *J. Am. Chem. Soc.* **1963**, *85*, 481.
(51) Fischer, E. O.; Breitschaft, S. *Angew. Chem.* **1963**, *75*, 94.
(52) King, R. B.; Bisnette, M. B. *Inorg. Chem.* **1964**, *3*, 785.
(53) Braunschweig, H.; Kupfer, T.; Lutz, M.; Radacki, K. *J. Am. Chem. Soc.* **2007**, *129*, 8993.
(54) Fortman, G. C.; Kégl, T.; Li, Q.-S.; Zhang, X.; Schaefer, H. F.; Xie, Y.; King, R. B.; Telser, J.; Hoff, C. D. *J. Am. Chem. Soc.* **2007**, *129*, 14388.
(55) Henc, B.; Jolly, P. W.; Salz, R.; Wilke, G.; Benn, R.; Hoffmann, E. G.; Mynott, R.; Schroth, G.; Seevogel, K.; Sekutowski, J. C.; Krüger, C. *J. Organomet. Chem.* **1980**, *191*, 425.
(56) Feng, H.; Wang, H.; Sun, Z.; Xie, Y.; King, R. B.; Schaefer, H. F. *J. Organomet. Chem.* **2010**, *695*, 2461.